



Nanostructured Carbide-Free Bainite Formation in Low Carbon Steel

Hamid Mousalou¹ · Sasan Yazdani¹ · Naghi Parvini Ahmadi¹ · Behzad Avishan²

Received: 9 January 2020 / Revised: 9 March 2020 / Accepted: 3 April 2020 / Published online: 23 June 2020
© The Chinese Society for Metals (CSM) and Springer-Verlag GmbH Germany, part of Springer Nature 2020

Abstract

It is an important challenge to reduce the carbon content in nanostructured bainitic steels for commercialization purposes while still being able to gain the desired microstructural characteristics in nanoscale and not to deteriorate the strength–ductility combinations. That is the point at which an appropriate heat treatment procedure design would be an important parameter. This article aims to investigate how to obtain nanostructured bainite in steel with 0.26 wt% carbon content by applying multi-step austempering procedures. One-, two- and three-step austempering processes have been implemented, and proper heat treatment temperatures and approaches were selected based on dilatometry tests. Results indicated that it has become possible to achieve bainitic ferrites and austenite films with overall thicknesses of 164, 145 and 132 nm and 134, 105 and 90 nm at the end of one-, two- and three-step austempering heat treatments, respectively. Meanwhile, microstructural characteristics resulted in enhanced mechanical properties with ultimate tensile strength (UTS) of 1435, 1455 and 1428 MPa in combination with elongation levels of 15.4, 13.6 and 11.4% after implementing those heat treatments. Finally, it has been shown that applying the multi-step austempering heat treatments resulted in enhanced yield strength and impact toughness values due to the microstructural characteristics and proper heat treatment procedure design.

Keywords Bainite · Multi-step austempering · Austenite · Mechanical properties · Impact toughness

1 Introduction

Nanostructured low-temperature carbide-free bainitic steels, with outstanding strength and ductility properties, have been developed recently which attained great interest among researchers due to their simple production method [1–12]. An appropriate chemical composition for these advanced materials can be primarily designed using phase transformation theories of steels [13–16] with no need for trial-and-error procedures and simulations, and a simple low-temperature austempering heat treatment (temperature range of 200–400 °C) gives the desired microstructural characteristics in nanoscale without any need to apply complicated shape deformation methods. Depending on the heat

treatment temperature, bainitic ferrites of less than 100 nm thicknesses can be achieved which is the main contributing factor in strength properties [16–18]. Considering the ductility, it is mainly depending on the volume fraction and morphology of the high-carbon retained austenite phase being present in the microstructure. Austenite presents in two filmy and blocky morphologies. The former separates the bainitic ferrites in each bainitic sheaf with identical thicknesses to that of bainitic ferrites, and the latter surrounds the sheaves. A high volume fraction of austenite is required for ductility promotion and replacement of austenite to martensite during straining the sample further adds to the resultant strength level due to the replacement of soft austenite with harder martensite [19, 20]. It has been approved that higher mechanical stability of austenite results in higher ductility since more gradual transformation to martensite occurs until later stages of failure [21].

Generally, there is no need to add any expensive alloying elements to the chemical composition to obtain desired mechanical performance or microstructural features and the total amount of alloying elements never exceeds more than 5 wt%. Meanwhile, carbon is the main alloying element in the composition which is added mainly to reduce

Available online at <http://link.springer.com/journal/40195>.

✉ Sasan Yazdani
yazdani@sut.ac.ir

¹ Faculty of Materials Engineering, Sahand University of Technology, P. O. Box: 51335/1996, Tabriz, Iran

² Department of Materials Engineering, Azarbaijan Shahid Madani University, Tabriz, Iran

the M_S temperature of the steel, making it possible to conduct the bainitic heat treatment at low temperatures. Almost 0.8–1 wt% carbon has been ordinarily used in different studies to achieve the desired mechanical and microstructural properties [6, 7, 22–27]. However, care must be taken to the point that a high amount of carbon would reduce the weldability of products which is of great concern for commercialization of nano-bainite. So it seems to be critical to reduce the carbon content as much as possible without deteriorating advanced properties.

There were some attempts to reduce the carbon content to less than 0.5 wt%, but they were accompanied with complicated production methods in some cases. Some studies applied ausforming procedures [28–30], and some implemented step austempering to compensate for the carbon reduction effect [31–33]. For instance, in an early attempt, Soliman et al. [31] carried out the two-step austempering on low carbon steel containing 0.26 wt% carbon and showed that two-step austempering resulted in a higher amount of bainite and lower volume fraction of retained austenite. Some tried to simply replace carbon with other alloying elements [34] to reduce the bainite transformation temperature and to compensate for the carbon reduction effect on M_S and B_S temperatures. However, it has been shown that coalescence bainitic ferrite has been formed at the end of the austempering heat treatment. In another attempt [35], the partial transformation of austenite to ferrite at an intermediate temperature range for hypoeutectoid steel resulted in carbon enrichment of remaining austenite before applying the austempering and its lower M_S temperature made it possible to obtain refined bainite in carbon-enriched austenite at lower temperatures. Such a heat treatment procedure would be effective for reducing the volume fraction and size of austenite blocks and additionally reducing the bainite plate thickness [35]. Finally, in previous research [36] using steel with similar alloying elements of this study but with lower Ni content, a significant improvement in impact toughness, enhancement of yield strength and formation of high-angle boundaries have been approved after conducting the multi-step austempering heat treatment.

According to the importance of the carbon reduction in nanostructured bainitic steels and considering the significance of designing a proper heat treatment procedure to obtain nanoscale bainite in low carbon steel, this article aims to study the possibility of attaining the desired mechanical and microstructural characteristics in steel with 0.26 wt% carbon. The steel composition has been designed using the bainite transformation theories, and proper substitutional alloying elements were used to compensate for the negative effect of carbon reduction on increasing the M_S and B_S temperatures.

2 Experimental

Primary steel with chemical composition of Fe–0.26C–0.96Mn–1.41Si–1.1Cr–3.1Ni–0.95Cu–0.25Mo–0.1V (all in wt%) was designed using the MUCG83™ thermodynamic model [37]. The significance of adding each alloying element can be found elsewhere [38]. According to which Si addition for preventing the cementite precipitation, Mo for preventing the temper embrittlement due to phosphorus, Mn, Ni and Cr for increasing the hardenability and preventing the formation of any diffusional phase formation and V for controlling the size of the primary austenite grains were inevitable. Steel was cast in an induction furnace under an inert gas atmosphere, and then, electro-slag remelting (ESR) process was carried out using Al_2O_3 –30%CaF₂ flux powder to obtain clean steel free from inclusions. The sample was hot-rolled to a sheet of 15 mm thickness after homogenizing at 1200 °C for 4 h. Dilatometry tests were performed to identify the critical temperatures of steel to design appropriate heat treatment cycles. Cylindrical specimens with 4 mm diameter and 10 mm length were machined from hot-rolled plate perpendicular to the rolling direction, and tests were performed using a Bahr Dil805A™ instrument with a heating rate of 5 °C/s and cooling rate of 20 °C/s. Practical test samples were fully austenitized at 900 °C for 20 min, and one-, two- and three-step austempering heat treatments were performed in salt bath furnaces.

Microstructural evaluations were implemented after grinding, polishing and etching the test materials using the standard procedure. Olympus PMG3™ optical microscope and Tescan MIRA3™ field emission gun scanning electron microscope were used, and various pictures at different high magnifications were selected to calculate the thicknesses of the bainitic ferrite plates and residual austenite films using the line intercept method [18, 39]. Because of the similarity of the morphology of austenite and martensite blocks in SEM images, samples were tempered at 200 °C for 2 h to reveal martensite when it was present.

X-ray diffraction was applied on heat-treated materials to measure the volume fraction of high-carbon retained austenite. Scanning was performed on samples using Brucker-D8 Advance™ diffractometer with $CuK\alpha$ radiation at 40 kV and 40 mA. Scanning was carried out in the range of 42–105° with 0.01 s⁻¹ scanning rate. The volume fraction of residual austenite was calculated using the integrated intensities of (200), (220) and (220) peaks of austenite and (200), (211) and (220) peaks of ferrite [40].

Hardness tests were implemented according to the ASTM E92-82 standard method using the HV30 scale, and reported values were the average of at least six measurements from different points of each sample. Flat tensile

test samples were prepared with gage lengths of 25 mm according to ASTM E8-09 standard method which were cut in the rolling direction. Tests were carried out on an Instron 8502™ tensile testing machine equipped with an extensometer using the 0.5 mm min^{-1} strain rate. At least three tests were performed for each heat treatment condition to ensure the reproducibility. $10 \text{ mm} \times 10 \text{ mm} \times 55 \text{ mm}$ Charpy impact test samples were prepared according to ASTM E23-07 standard in which notches were perpendicular to the rolling direction. At least four tests at each heat treatment condition were performed at room temperature using Roell Amsler™ impact testing instrument.

3 Results and discussion

Figure 1 illustrates the dilatometry test results whereby A_{C1} , A_{C3} and M_{S1} temperatures of the primary material have been determined to be 710, 812 and 295 °C, respectively (Fig. 1a, b). Accordingly, samples were categorized in three sets of one-step, two-step and three-step austempering specimens and the bainitic transformation was carried out at 315 °C, almost 20 °C above the experimentally determined M_{S1} temperature during the ordinary one-step heat treatment process. It was also crucial to determine the optimum heat treatment time at which bainitic transformation completed at 315 °C to be sure to gain the maximum volume fraction of bainite. For this aim, samples were austenitized at 930 °C, above the determined A_{C3} temperature and rapidly cooled to 315 °C and allowed the bainite transformation to be completed. The optimum heat treatment time has been determined to be almost 90 min at which the dilatometry curve reached a plateau, as it is evident in Fig. 1c. Accordingly, practical one-step austempering heat treatment has been carried out in salt bath furnaces and samples were austenitized at 900 °C for 20 min and then quenched to 315 °C immediately holding for 4 h to obtain the desired microstructure. Heat treatment

time was selected longer than 90 min because of the bigger sizes of the experimental test samples compared to that of dilatometry test specimens. This would ensure the bainite transformation completion at 315 °C.

Two- and three-step austempering heat treatments were carried out after partial bainite transformation at 315 °C. For this aim, samples were partially transformed to bainite during the first stage at 315 °C until 75% of maximum bainite content formed. This made the remaining austenite richer in carbon because of the carbon partitioning from bainitic ferrite formed during the first step. So it was logical to have a lower M_S temperature of retained austenite comparing to that of raw material. Therefore, samples were analyzed again by dilatometry tests to determine the time at which 75% of bainite formed and the M_S temperature of remaining austenite at the end of partial transformation as it is shown in Fig. 2. Dilatometry sample was rapidly cooled down at the rate of 20 °C/s to 315 °C after complete austenitization at 930 °C for 15 min and then held at that temperature for 28 min to gain 75% maximum bainitic content. Immediately after, samples were cooled down to room temperature at the rate of 20 °C/s. Results indicated that M_{S2} temperature was nearly 246 °C for remaining austenite at the end of the partial bainite transformation. Accordingly, the bainitic transformation temperature of the second step was selected as 260 °C, being almost 14 °C above the determined M_{S2} . Practical two-step thermal cycle included samples austenitization at 900 °C for 20 min, partial bainite transformation at 315 °C for 28 min followed by quenching to 260 °C and holding for 22 h and immediately cooling down to room temperature. Optimum heat treatment time for the second step of austempering has been selected using the kinetics test samples. The three-step thermal cycle also included samples austenitization at 900 °C for 20 min, partial austempering at 315 °C for 28 min, fast cooling to 260 °C and holding for 22 h, fast cooling to 200 °C and holding for 54 h and finally cooling down to room temperature. Figure 3

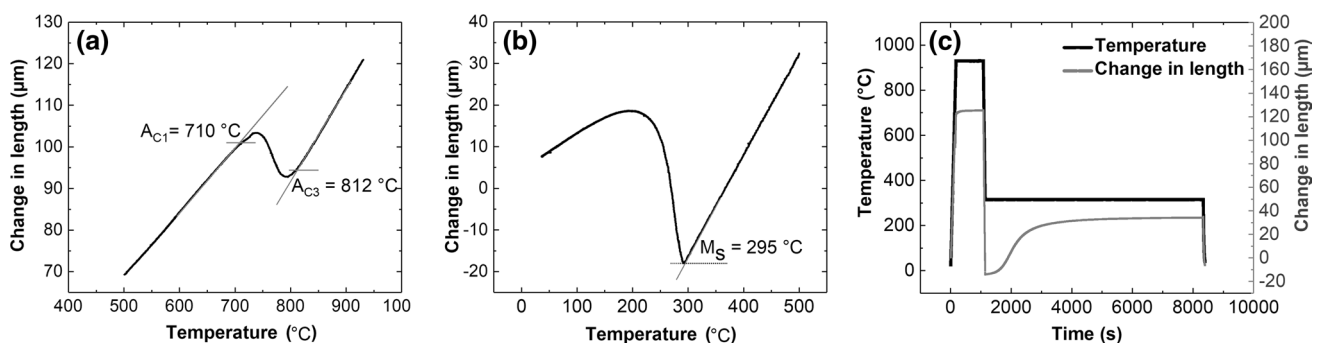


Fig. 1 Dilatometry curves **a** to measure the A_{C1} and A_{C3} temperatures and **b** to measure the M_{S1} temperature, **c** thermal cycle and dilatation curves showing the kinetics of bainitic transformation at 315 °C

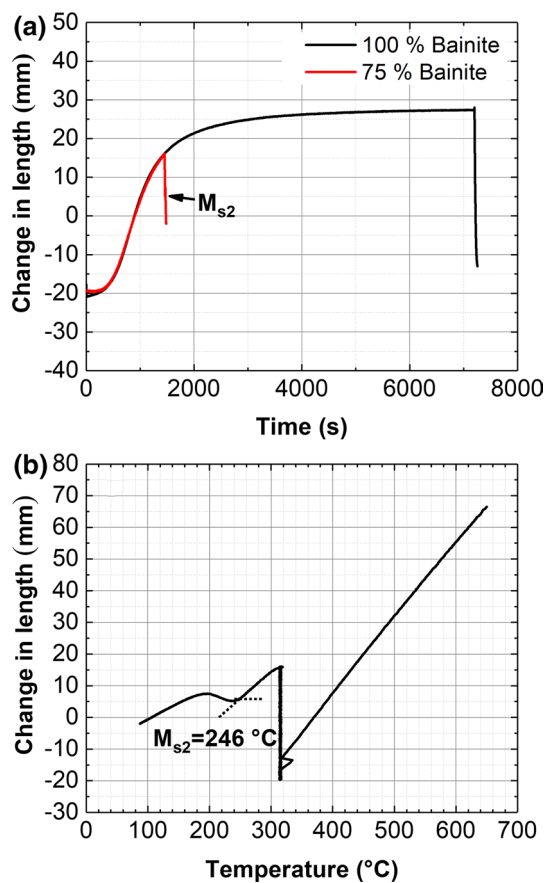


Fig. 2 Dilatometry curves **a** to determine the time at which almost 75% bainite formed at 315 °C and **b** to measure martensite start temperature for remaining austenite (M_{s2}) being present at the end of partial bainite transformation

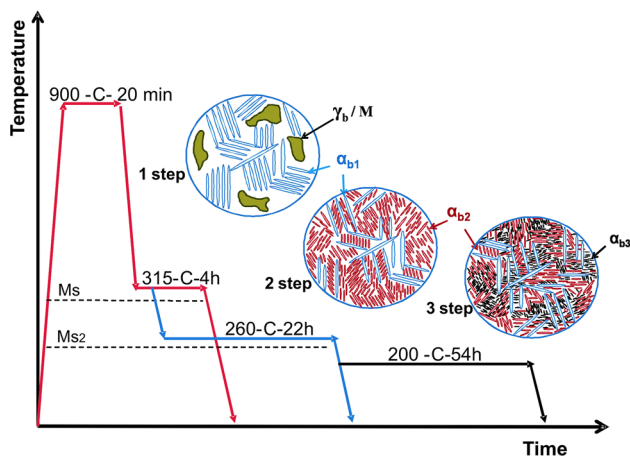


Fig. 3 One-, two- and three-step austempering heat treatment cycles as well as anticipated microstructural features during the heat treatment procedures. γ_b , M , α_{b1} , α_{b2} and α_{b3} represent austenite blocks, martensite, bainitic ferrite formed at the first step, bainitic ferrite formed at the second step and bainitic ferrite formed at the third step, respectively

summarizes the heat treatment procedures designed based on dilatometry tests, and anticipated microstructural changes have been shown.

Figure 4 depicts the microstructural characteristics of different materials at the end of the various heat treatment procedures performed in salt bath furnaces. It is evident that all samples mainly transformed to bainite and austenite micro-blocks separated the bainitic sheaves. Furthermore, some martensite could also be detected within the microstructure.

Considering the one-step austempering condition (Fig. 4a), it was obvious that bainitic sheaves were separated with austenite microblocks and each sheaf consisted of parallel layers of bainitic ferrites and austenite films. Carbon rejects from bainitic ferrites to surrounding austenite during the bainite transformation and bainite formation stops when austenite carbon content reaches to that of predicted by T_0 diagram [38]. Accordingly, austenite films are expected to be more enriched in carbon comparing to that of austenite blocks, the latter being especially poor in carbon in center regions. It has been shown that this would result in higher thermal and mechanical stability of filmy morphology comparing to that of blocky austenites [41, 42]. That is the reason why center regions of austenite blocks are prone to transform to martensite during cooling to room temperature at the end of the bainite transformation.

Figure 4b, c depicts the microstructural characteristics of samples after two- and three-step austempering heat treatment procedures, respectively, and Fig. 4d shows the high-magnification image of the white square in Fig. 4c indicating the thickness of bainitic ferrite plates separated relatively with long austenite films. Results indicated that the lower volume fraction of austenite blocks with smaller mean diameters was attained at the end of the step austempering heat treatment processes comparing to that of achieved in ordinary one-step austempering. Moreover, it can be seen that step austempering further refined the overall size of the bainitic ferrites and austenite films.

Microstructural characteristics can be justified according to the fact that thermally less stable big austenite blocks being present at the end of the first step further decomposed to bainite during the second and third heat treatment stages at lower transformation temperatures. That is the reason why lower volume fractions and smaller austenite blocks were achieved at the end of the step austempering processes. Precise microstructural evaluations indicated that the mean diameter of austenite blocks decreased from 1600 ± 520 nm in the one-step austempering sample to almost 740 ± 120 nm and 710 ± 100 nm in two- and three-step heat treatment cycles, respectively. On the other hand, since the austempering temperature was lower during the second and third steps, it was logical to gain finer bainitic ferrite and austenite films considering the average size knowing that their thicknesses are mainly depending on the heat treatment temperature and

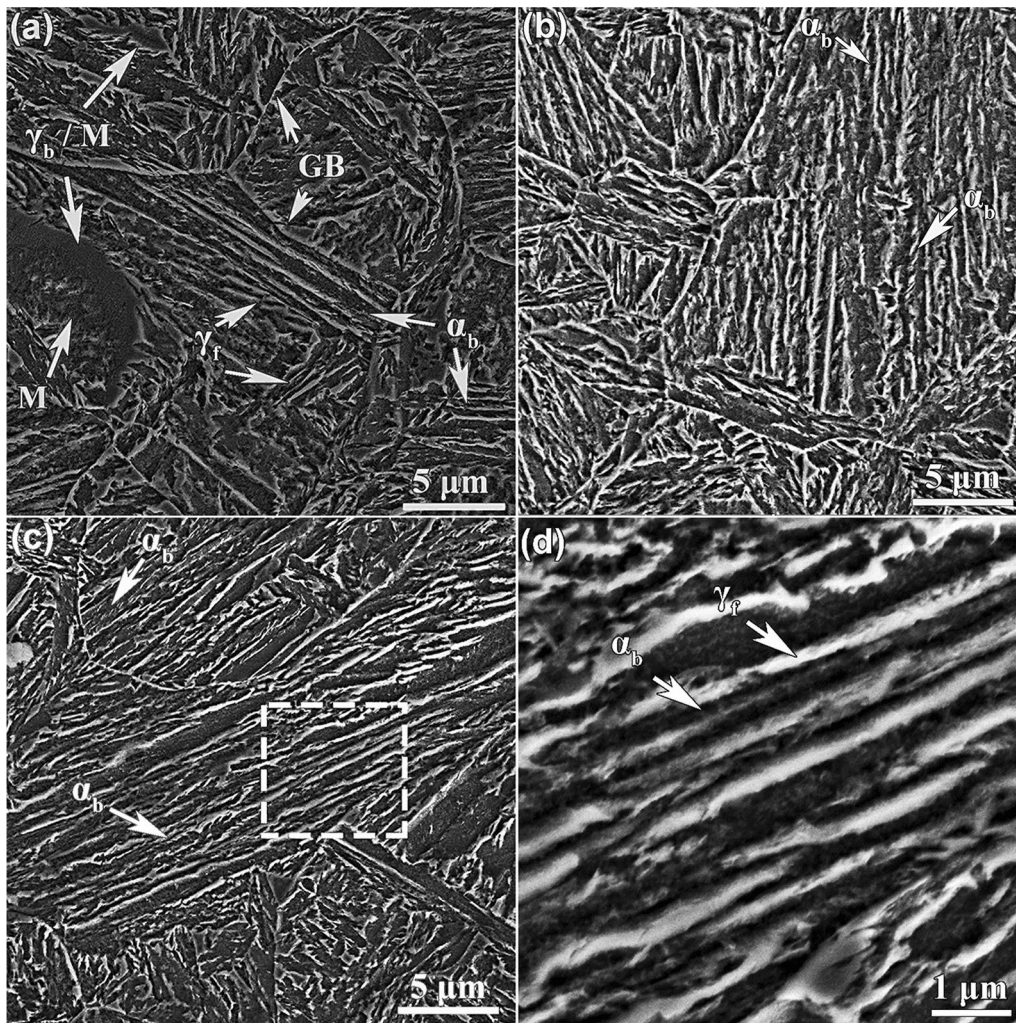


Fig. 4 SEM micrographs of **a** one-step, **b** two-step, **c** three-step austempering samples and **d** high-magnification image of the selected region in **c**. GB, γ_b , γ_f , M and α_b represent prior austenite grain boundary, austenite blocks, austenite films, martensite and bainitic ferrite, respectively

strength of the austenite in which bainite forms [43]. Austenite was stronger at lower transformation temperatures, and increasing the austenite strength further decreased the thicknesses of the bainitic subunits and austenite films. Apart from the effect of temperature on strength of austenite, this phase became more enriched in carbon at the end of the first step and its carbon content increased compared to the parent austenite. Similarly, the second step austempering further saturated the austenite from which bainitic ferrites and austenite films formed. This made austenite much stronger, and it resisted the motion of the glissile interface of ferrite–austenite considerably that resulted in more refined microstructure. As a result, it was not strange to see a wider size distribution of bainitic ferrites and austenite films at the end of the step austempering comparing to that of ordinary one-step heat treatment. Implementing the step austempering resulted in the formation of finer bainitic ferrites and austenite films during every other step comparing to the

previous heat treatment step. Similarly, bainite formed at the end of the third stage was much refined comparing to that of the other two heat treatment procedures. Figure 5 shows the very fine bainitic ferrites and austenite films with almost less than 100 nm thicknesses which may form at the end of the third step of heat treatment.

Figure 6 illustrates the size distributions of bainitic ferrite plates at the end of each heat treatment procedure. Results indicated that one-step austempering ended in the narrowest size distribution, while applying two- and three-step heat treatments gave wider size distributions being more considerable after three-step austempering. Additionally, analytic evaluations indicated that overall finer microstructure could be achieved after multi-step austempering heat treatment procedures due to thinner microstructural constituents formed during every other heat treatment steps. It is not strange to observe a similar trend for austenite films' sizes and distributions as it is shown in Fig. 7. This can be

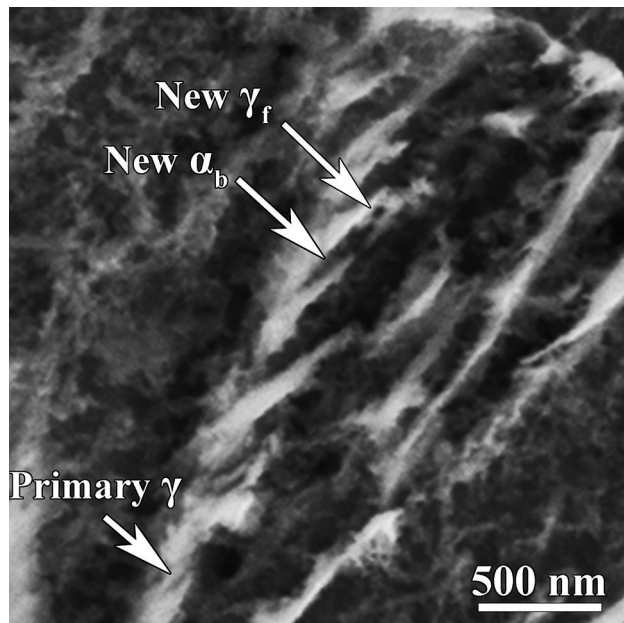


Fig. 5 Nanoscale bainitic ferrites and austenite films formed at the end of the third step of austempering heat treatment

justified according to the fact that austenite films would have almost identical sizes to those of bainitic ferrite subunits within bainitic sheaves. Thicker bainitic ferrites would partition a higher amount of carbon to longer distances in front of the austenite–ferrite interface [39]. So knowing that the bainite transformation would stop when the carbon content reaches to that of predicted by T_0 diagram [39, 44], it is logical to gain thicker austenite films when thicker bainitic ferrites form.

The amount of bainite formed would affect the volume fraction of high-carbon retained austenite within the microstructure. This is evident in Fig. 8 which shows the X-ray diffraction patterns of the samples at the end of each heat treatment procedure. Results indicated that samples contained two main austenite and ferrite phases for which different peak intensities could be detected. Quantitative data from XRD refinement are summarized in Fig. 9 and approved that performing two- and three-step austempering heat treatments resulted in the reduction of retained austenite within the microstructure. That is because of the further decomposition of austenite blocks to bainite at every other

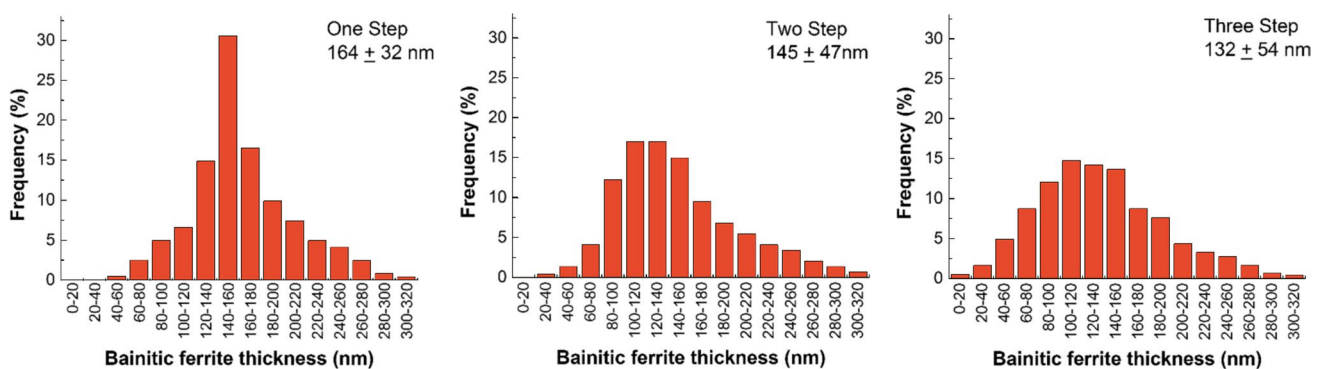


Fig. 6 Mean thicknesses and size distributions of bainitic ferrite plates at the end of different heat treatment conditions

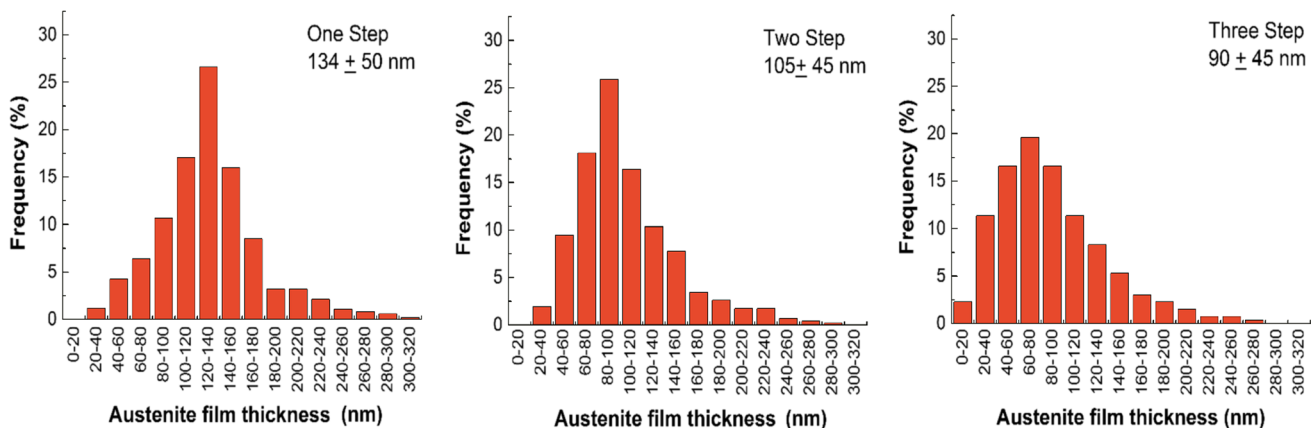


Fig. 7 Mean thicknesses and size distributions of austenite films at the end of different heat treatment conditions

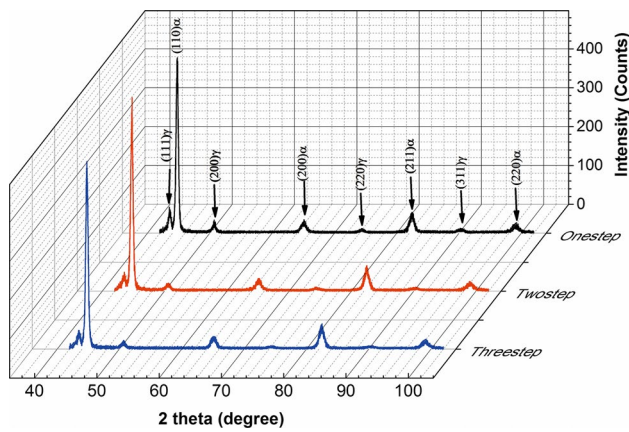


Fig. 8 XRD patterns of samples after one-, two- and three-step austempering heat treatments

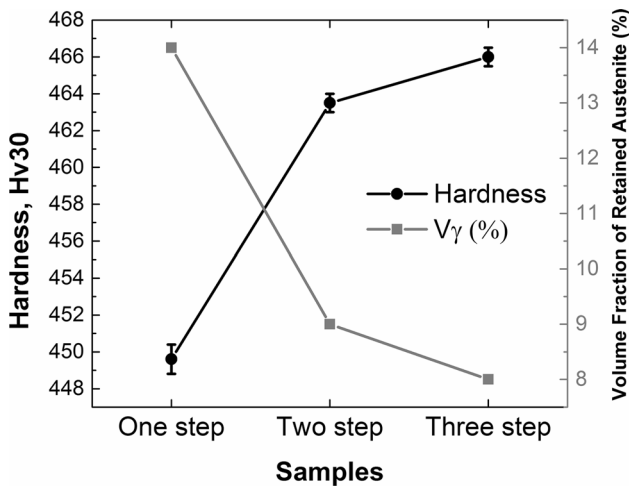


Fig. 9 Changes in hardness values and the volume fraction of retained austenite after one-, two- and three-step austempering heat treatments

stage by applying multi-step austempering heat treatment. Austenite content decreased from almost 14% in single-step austempering to almost 8% in three-step isothermal bainite heat treatment. As a result, it was logical to assume to have various hardness values due to the microstructural changes in different heat-treated samples. As it is shown in Fig. 9, samples were harder in multi-step austempering cases because of the replacement of soft austenite phase with harder bainitic ferrites and increasing the volume fraction of bainite further enhanced the hardness value.

Mechanical properties in heat-treated specimens would also be affected by microstructural changes, and different strength–ductility combinations were predicted at the end of different heat treatment cycles. Figure 10 gives the engineering stress–strain curves according to which a continuous yielding during the transition from elastic to plastic region

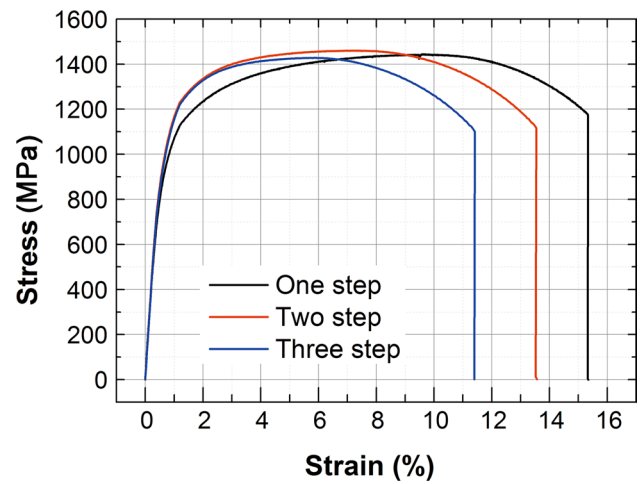


Fig. 10 Engineering stress–strain curves for heat-treated materials

Table 1 Yield strength (YS), ultimate tensile strength (UTS) and elongation (EL) values at the end of different heat treatment procedures

Heat treatment procedure	YS (MPa)	UTS (MPa)	EL (%)
One-step austempering	895 ± 20	1435 ± 5	15.4 ± 0.5
Two-step austempering	1016 ± 10	1455 ± 10	13.6 ± 1
Three-step austempering	1000 ± 15	1428 ± 10	11.4 ± 1

could be spotted which can be explained due to the presence of free dislocations in microstructure because of the shear transformation mechanism of bainite transformation [45]. Quantitative data were also summarized in Table 1 extracted from the stress–strain curves. Results indicated that performing two- and three-step austempering heat treatments successfully increased the yield strength values even if there was not a significant change in ultimate tensile strength level. Moreover, it can be seen that elongation decreased by applying step austempering heat treatments, but it was not that much considerable and still an acceptable strength–ductility combination could be obtained. Strength properties are mainly controlled by volume fraction and size of the bainitic ferrites, while ductility is depending on the volume fraction of the high-carbon retained austenite present within the microstructure [21, 45]. The higher volume fraction of finer bainitic ferrites will increase the strength level, and a higher amount of austenite is demanded to gain higher elongation level. That is the reason for achieving higher yield strength level in multi-step austempering heat treatment conditions and higher uniform elongation in the case of single-step austempering.

Figure 11 elucidates the impact toughness variations after applying different heat treatment procedures. It can be seen that higher impact toughness values could be reached in step

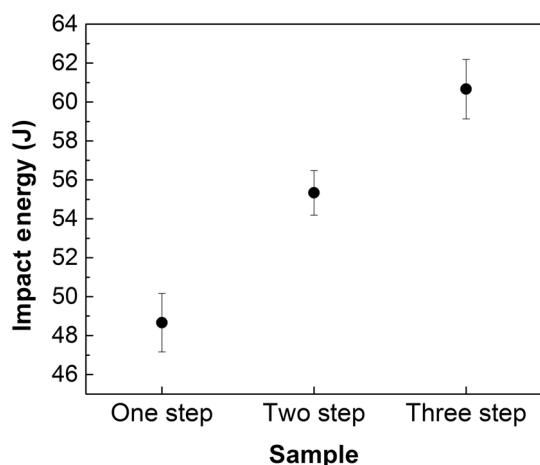


Fig. 11 Toughness variations after applying different heat treatment procedures

austempering conditions and the maximum value achieved for the three-step bainitic heat treatment procedure. Results can be justified considering that not only the volume fraction of retained austenite and also its morphology are important factors when considering the impact toughness in carbide-free bainitic microstructures [46]. The priority is to gain higher impact toughness when a higher amount of austenite is present within the microstructure. However, previous studies approved that the lower volume fraction of blocky austenite and smaller blocks are mandatory to attain higher impact toughness level [46]. Austenite blocks are mechanically less stable comparing to austenite films, and it is vital to replace blocky morphology with filmy austenites if higher toughness values are demanded. Additionally, the presence of bainitic plates with different crystallographic orientations would be more effective in crack deflection. Bainitic sheaves propagated in different directions successfully arrest the crack growth and increase the material's resistance to crack progress [47]. In this case, multi-step austempered materials with a lower amount and smaller austenite blocks and more bainitic sheaves propagated in different directions would give improved impact toughness values.

Figure 12 shows the fracture surfaces of the impact test samples for all three heat treatment conditions. It is evident that fracture surfaces are composed of both ductile fracture regions with fine dimples and brittle regions with quasi-cleavage facets. The latter was much evident in the one-step austempering sample due to the presence of coarse austenite/martensite blocks. Large blocks of retained austenite caused

fast crack propagation by early strain-induced martensite formation during straining the material [48]. However, implementing two- and three-step austempering heat treatments reduced the volume fraction of big austenite blocks and increased the amount of mechanically more stable austenite films within the microstructure which consequently resulted in much ductile fracture mode.

4 Conclusions

It is the key point to reduce the carbon content in nanostructured bainitic steels for commercialization purposes. At the same time, it would be essential to design an appropriate heat treatment procedure to compensate for the carbon reduction effect. Step austempering has been carried out on steel with 0.26 wt% carbon in this study, and dilatometry tests have been used to design the proper heat treatment processes.

One-step (315 °C-4 h), two-step (315 °C-28 min/260 °C-22 h) and three-step (315 °C-28 min/260 °C-22 h/200 °C-54 h) heat treatments have been applied, and partial transformation of austenite to martensite has been occurred before starting every other stage of austempering. Results indicated that it has become possible to gain much finer nanoscale bainitic ferrites and austenite films and smaller austenite blocks at the end of step austempering heat treatments which resulted in strength–ductility combinations similar to that of ordinary high-carbon nano-bainite. Bainitic ferrites of 164, 145 and 132 nm and austenite films of 134, 105 and 90 nm thicknesses could be achieved at the end of one-, two- and three-step heat treatments, respectively. Big austenite blocks further decomposed to bainite at every other stage, and mean sizes of the blocks reduced from 1600 nm in ordinary one-step heat treatment to 710 nm at the end of three-step austempering. Microstructural refinement ended in higher yield strengths for step austempered samples and UTS levels of 1435, 1455 and 1428 MPa in combination with elongation values of almost 15.4, 13.6 and 11.4% could be obtained, respectively. Moreover, it has been observed that wider size distributions of bainitic subunits and austenite films could be attained after implementing the two- and three-step austempering and microstructural characteristics ended in higher hardness and improved impact toughness values comparing to that of ordinary one-step heat treatment.

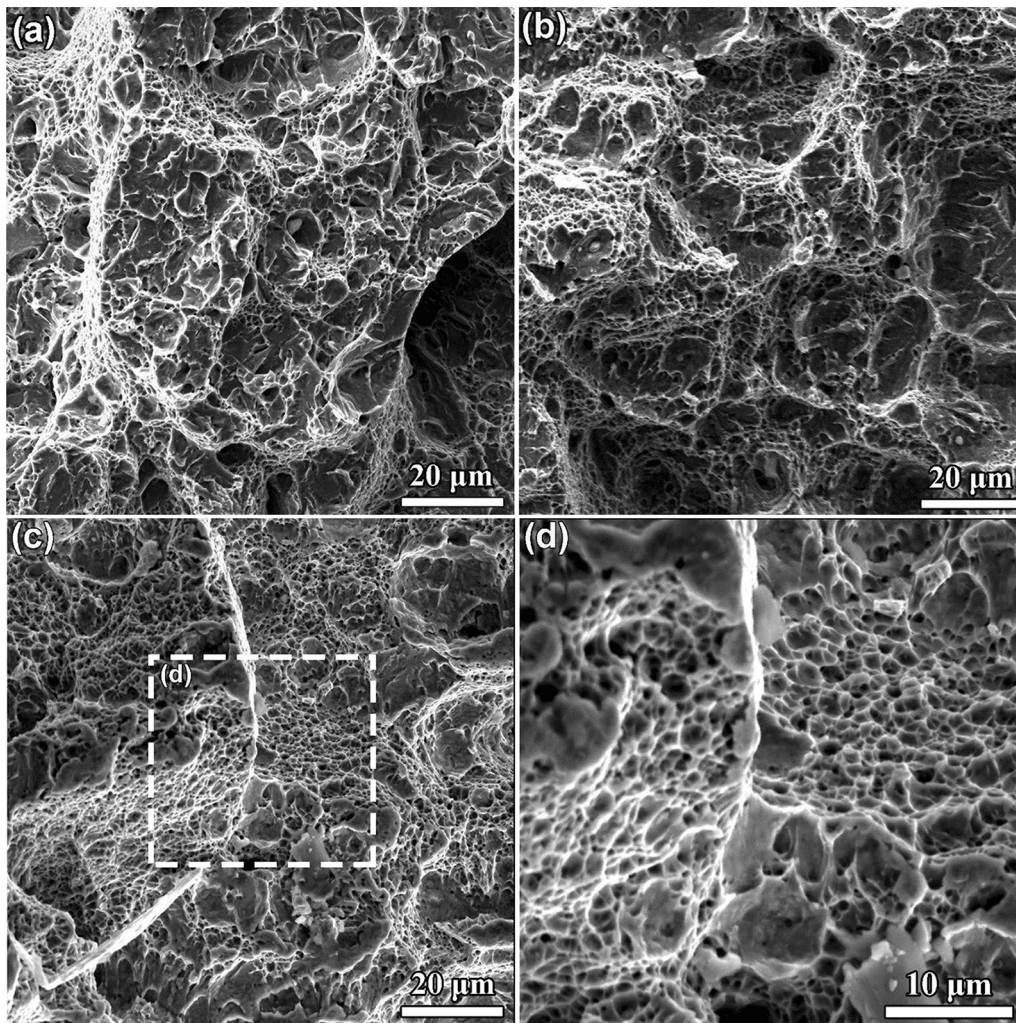


Fig. 12 SEM images of fracture surfaces of impact test samples subjected to **a** one-step, **b** two-step, **c** three-step austempering heat treatment conditions, **d** high-magnification image from the rectangular region in **c**

References

- [1] C. García Mateo, F.G. Caballero, H.K.D.H. Bhadeshia, *ISIJ Int.* **43**, 1238 (2003)
- [2] H.K.D.H. Bhadeshia, P. Brown, C. Garcia-Mateo, Patent No. GB2462197 (2010)
- [3] I. Mueller, R. Rementeria, F. Caballero, M. Kuntz, T. Sourmail, E. Kerscher, *Materials* **9**, 831 (2016)
- [4] H. Huang, M. Sherif, P. Rivera-Díaz-del-Castillo, *Acta Mater.* **61**, 1639 (2013)
- [5] A. Polishetty, C. Sonavane, P. Patil, G. Littlefair, *J. Mater. Sci. Chem. Eng.* **2**, 34 (2014)
- [6] F.G. Caballero, C. Garcia-Mateo, M.K. Miller, *JOM* **66**, 747 (2014)
- [7] H.S. Hasan, M.J. Peet, M.N. Avettand-Fènoël, H.K.D.H. Bhadeshia, *Mater. Sci. Eng. A* **615**, 340 (2014)
- [8] J. Zhao, T. Wang, B. Lv, F. Zhang, *Mater. Sci. Eng. A* **628**, 327 (2015)
- [9] J. Yang, T. Wang, B. Zhang, F. Zhang, *Wear* **282**, 81 (2012)
- [10] Y. Tsai, C. Lin, W. Lee, C. Huang, J. Yang, *Scr. Mater.* **115**, 46 (2016)
- [11] I. Timokhina, H. Beladi, X. Xiong, Y. Adachi, P. Hodgson, *Acta Mater.* **59**, 5511 (2011)
- [12] Y. Huang, A.M. Zhao, J.G. He, X.P. Wang, Z.G. Wang, L. Qi, *Int. J. Miner. Metall. Mater.* **20**, 1155 (2013)
- [13] F.G. Caballero, M.J. Santofimia, C. Capdevila, C. García-Mateo, C. García de Andrés, *ISIJ Int.* **46**, 1479 (2006)
- [14] C. Garcia-Mateo, F.G. Caballero, *Int. J. Mater. Res.* **98**, 137 (2007)
- [15] H.K.D.H. Bhadeshia, R.W.K. Honeycombe, *Steels: microstructure and properties*, 4th edn. (Butterworth-Heinemann, 2017)
- [16] T. Yokota, C. García Mateo, H.K.D.H. Bhadeshia, *Scr. Mater.* **51**, 767 (2004)
- [17] M.N. Yoozbashi, S. Yazdani, *Mater. Sci. Eng. A* **527**, 3200 (2010)
- [18] C. García Mateo, F.G. Caballero, H.K.D.H. Bhadeshia, *ISIJ Int.* **43**, 1821 (2003)
- [19] H.K.D.H. Bhadeshia, D.V. Edmonds, *Met. Sci.* **17**, 411 (1983)
- [20] H.K.D.H. Bhadeshia, D.V. Edmonds, *Met. Sci.* **17**, 420 (1983)
- [21] B. Avishan, S. Yazdani, F. Caballero, T. Wang, C. Garcia-Mateo, *Mater. Sci. Technol.* **31**, 1508 (2015)
- [22] H. Amel-Farzad, H. Faridi, F. Rajabpour, A. Abolhasani, S. Kazemi, Y. Khaledzadeh, *Mater. Sci. Eng. A* **559**, 68 (2013)

- [23] H. Lan, L. Du, N. Zhou, X. Liu, *Acta Metall. Sin. Engl. Lett.* **27**, 19 (2014)
- [24] C. Garcia-Mateo, J. Jimenez, H.-W. Yen, M. Miller, L. Morales-Rivas, M. Kuntz, S. Ringer, J.-R. Yang, F. Caballero, *Acta Mater.* **91**, 162 (2015)
- [25] Y. Tsai, H. Chang, B. Huang, C. Huang, J. Yang, *Mater. Charact.* **107**, 63 (2015)
- [26] K. Fang, J. Yang, K. Song, X. Liu, Z. Dong, H. Fang, *Met. Mater. Int.* **20**, 923 (2014)
- [27] K. Rakha, H. Beladi, I. Timokhina, X. Xiong, S. Kabra, K.D. Liss, P. Hodgson, *Mater. Sci. Eng. A* **589**, 303 (2014)
- [28] M. Zhang, Y. Wang, C. Zheng, F. Zhang, T. Wang, *Mater. Des.* **62**, 168 (2014)
- [29] A. Eres-Castellanos, L. Morales-Rivas, A. Latz, F.G. Caballero, C. Garcia-Mateo, *Mater. Charact.* **145**, 371 (2018)
- [30] G. Chen, G. Xu, H. Hu, J. Tian, Q. Yuan, J. Wang, *Mater. Res. Express.* **7**, 016519 (2020)
- [31] M. Soliman, H. Mostafa, A.S. El-Sabbagh, H. Palkowski, *Mater. Sci. Eng. A* **527**, 7706 (2010)
- [32] X. Wang, K. Wu, F. Hu, L. Yu, X. Wan, *Scr. Mater.* **74**, 56 (2014)
- [33] J. Tian, G. Xu, Z. Jiang, M. Zhou, H. Hu, Q. Yuan, *ISIJ Int.* **58**, 1875 (2018)
- [34] H.S. Yang, H.K.D.H. Bhadeshia, *Mater. Sci. Technol.* **24**, 335 (2008)
- [35] M. Soliman, H. Palkowski, *ISIJ Int.* **47**, 1703 (2007)
- [36] H. Mousalou, S. Yazdani, B. Avishan, N.P. Ahmadi, A. Chabok, Y. Pei, *Mater. Sci. Eng. A* **734**, 329 (2018)
- [37] H.K.D.H. Bhadeshia, Materials Algorithms Project. <https://www.msm.cam.ac.uk/map/steel/programs/mucg83.html>
- [38] H.K.D.H. Bhadeshia, *Bainite in Steels*, 2nd edn. (Institute of Materials, London, 2001)
- [39] L.C. Chang, H.K.D.H. Bhadeshia, *Mater. Sci. Technol.* **11**, 874 (1995)
- [40] B.D. Cullity, S.R. Stock, *Elements of X-ray diffraction* (Prentice-Hall Inc, New York, 2001)
- [41] K.W. Kim, K.I. Kim, C.H. Lee, J.Y. Kang, T.H. Lee, K.M. Cho, K.H. Oh, *Mater. Sci. Eng. A* **673**, 557 (2016)
- [42] N. Van Dijk, A. Butt, L. Zhao, J. Sietsma, S. Offerman, J. Wright, S. Van der Zwaag, *Acta Mater.* **53**, 5439 (2005)
- [43] S.B. Singh, H.K.D.H. Bhadeshia, *Mater. Sci. Eng. A* **245**, 72 (1998)
- [44] Z. Ławrynowicz, S. Dymski, *Adv. Mater. Sci.* **8**, 80 (2008)
- [45] B. Avishan, C. Garcia-Mateo, L. Morales-Rivas, S. Yazdani, F.G. Caballero, *J. Mater. Sci.* **68**, 6121 (2013)
- [46] B. Avishan, S. Yazdani, S.H. Nedjad, *Mater. Sci. Eng. A* **548**, 106 (2012)
- [47] S. Golchin, B. Avishan, S. Yazdani, *Mater. Sci. Eng. A* **656**, 94 (2016)
- [48] X. Long, F. Zhang, J. Kang, B. Lv, X. Shi, *Mater. Sci. Eng. A* **594**, 344 (2014)